Reduction of Facet Reflectivity of Quantum-Cascade Lasers With Subwavelength Gratings

Afusat O. Dirisu, *Student Member, IEEE*, Grace Silva, Zhijun Liu, *Student Member, IEEE*, Claire F. Gmachl, *Senior Member, IEEE*, Fred J. Towner, John Bruno, and Deborah L. Sivco

***Abstract*—We demonstrate the reduction of the facet reflectivity of quantum-cascade lasers (QCLs) by using subwavelength gratings. The gratings were fabricated on $\lambda = 4.9$- and 9.8-μm QCLs using focused ion beam milling. Reflectivities as low as 1%–3% for the 4.9-μm QCL and as low as 4%–8% for the 9.8-μm QCL are reported.**

***Index Terms*—Antireflection (AR), grating, midinfrared, quantum-cascade lasers (QCLs).**

I. Introduction

QUANTUM-CASCADE lasers (QCLs) and other semiconductor lasers usually use cleaved end-facets for feedback. The facet reflectivity for most III–V semiconductors is around 30%. Reduction of this reflectivity is necessary to increase the performance of lasers used as distributed feedback lasers [1], in external cavity mode [2], [3], and as superluminescent light-emitting diodes [4]. Currently, antireflection (AR) coatings of single or multilayer are deposited on the facet(s) to reduce the reflectivity. In the midinfrared region, where most QCLs emit, the AR coatings are thicker and adhesion to the facet can be a problem due to built-in stress. Also, during operation, QCLs may undergo thermal cycling which in turn can result in the eventual delamination of the coating from the facet.

Here, we demonstrate an alternative to AR coatings, namely subwavelength gratings, fabricated directly on the laser facet. Since the gratings are monolithic with the laser, we avoid the problems mentioned above. The subwavelength grating parameters were calculated using thin-film theory (TFT) and effective medium theory (EMT) [5]–[8] and were fabricated with a focused beam of Ga+ ions. The lasers were characterized before and after milling by measuring the light–current–voltage (L–I–V) and spectral characteristics. The measured residual reflectivity of the AR facets was determined from the measured change in threshold current density and slope efficiency.

Manuscript received October 6, 2006; revised December 6, 2006. This work was supported in part by National Science Foundation (NSF)-DMR-0213706 through Princeton University MRSEC PCCM, in part by NSF Grant EEC-0540832 (MIRTHE-ERC), and in part by Defense Advanced Research Projects Agency (DARPA) L-PAS.

A. O. Dirisu, Z. Liu, and C. F. Gmachl are with the Department of Electrical Engineering, Princeton University, Princeton, NJ 08544 USA (e-mail: adirisu@princeton.edu).

G. Silva was with the Department of Electrical Engineering, Princeton University, Princeton, NJ 08544 USA. She is now with the Department of Biological Sciences, University of Maryland Baltimore County, Baltimore, MD 21250 USA.

F. J. Towner and J. Bruno are with Maxion Technologies, Hyattsville, MD 20782 USA.

D. L. Sivco is with Lucent Technologies, Murray Hill, NJ 07974 USA.

Digital Object Identifier 10.1109/LPT.2006.890755

II. Theory

In subwavelength gratings, only the zeroth-order reflected and transmitted waves are allowed to propagate since the wavelength λ of the incident radiation is long compared to the grating period Λ of the structure, i.e., $\Lambda/\lambda \to 0$. As such, the subwavelength grating structure acts as a homogeneous medium with a single effective index of refraction determined by the filling factor, i.e., the ratio of the grating ridge width to the grating period. The effective index is also dependent on the polarization of the incident electric field with respect to the orientation of the grating [6]. From the first-order EMT, the effective permittivity is defined as [7], [8]

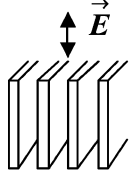

$$\varepsilon_{\parallel}^{(0)} = (1-f)n_1^2 + fn_2^2 \tag{1a}$$

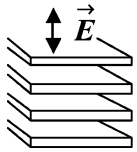

$$\varepsilon_{\perp}^{(0)} = \left[\frac{(1-f)}{n_1^2} + \frac{f}{n_2^2}\right]^{-1} \tag{1b}$$

where $\varepsilon_{\parallel}$ and $\varepsilon_{\perp}$ are the effective permittivities of the grating structure for the electric field parallel (vertical gratings) and perpendicular (horizontal gratings) to the grooves, respectively, f is the filling factor, n_1 and n_2 are indexes of the grooves and ridges of the gratings, respectively. The equation for higher order EMT permittivity is given in [8].

In TFT, the reflectivity of a film is determined by the Fresnel coefficients at the interface of the film and its surrounding media and is given as [5], [6]

$$R = \frac{r_{1f}^2 + r_{f2}^2 + 2r_{1f}r_{f2}\cos(2k_0 n_f t_f \cos\theta_2)}{1 + r_{1f}^2 r_{f2}^2 + 2r_{1f}r_{f2}\cos(2k_0 n_f t_f \cos\theta_2)} \tag{2}$$

where θ_2 is the transmitted angle of the incident wave in the film, r_{1f} and r_{f2} are the reflection coefficients at the incident and transmitted interfaces, respectively. At normal incidence, the condition of zero reflectivity results in an index of refraction n_f and thickness t_f

$$n_f = \sqrt{n_1 n_2} \tag{3a}$$

$$t_f = m\lambda_0/4n_f, \qquad m = 1, 2, 3, \ldots \tag{3b}$$

Combining EMT and TFT by inserting n_f in (3a) into (1a) or (1b), the filling factor that will result in an AR structure with grating depth t_f, is determined. For our QCLs, $n_2 \approx 3.17$ and

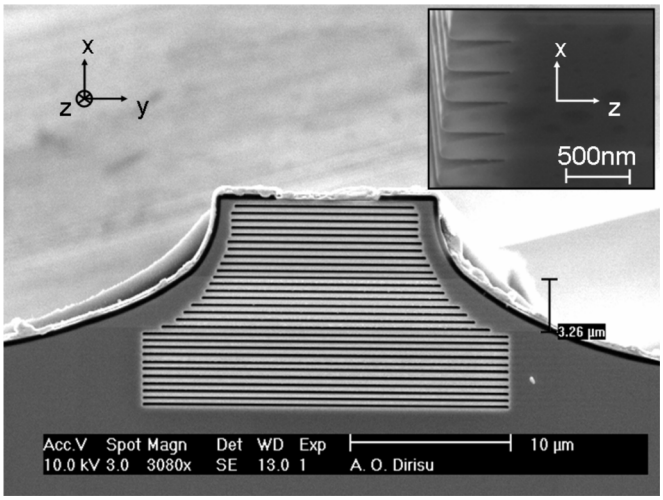

Fig. 1. Scanning electron microscope (SEM) image of a QCL facet milled with horizontal gratings. The inset shows a cross section of the gratings along the length of the laser ridge (the z direction).

$n_1 = 1.0$; hence, n_f is 1.79 and f is 0.76 (0.24) for horizontal (vertical) gratings.

The reflectivity of the facet can be determined from the threshold current density $J_{\rm th}$ or the slope efficiency of the output light dL/dI

$$J_{\rm th} = (1/2L_{\rm cav}g\Gamma)\left[2L_{\rm cav}\alpha_w - \ln(R_{m1}R_{m2})\right] \quad (4a)$$

$$dL/dI = (\zeta/2L_{\rm cav}) \times \{\ln R_{m1}/\left[\ln(R_{m1}R_{m2}) - 2L_{\rm cav}\alpha_w\right]\} \quad (4b)$$

where $L_{\rm cav}$ is the length of the laser ridge, α_w the waveguide loss, Γ the confinement factor, g the gain coefficient, R_{m1} and R_{m2} are the power reflectivities of the front and back facets, and ζ is proportional to the internal efficiency of the laser [9].

III. Experiment

The gratings were fabricated into the front facet of the QCLs using an FEI strata DB-235 focused ion beam (FIB) system with Ga^+ liquid metal ion source. The ion beam is accelerated at an energy of 30 KeV, focused onto the surface of the facet and raster scanned in the areas to be milled. The high filling factor of the horizontal gratings, as compared to vertical gratings, results in less material to be milled which shortens processing time and reduces the facet exposure to the ion beam. An example of a milled 9.8-μm QCL facet is shown in Fig. 1.

The lasers were characterized in pulsed mode at 79-KHz repetition rate and 100-ns pulsewidth for spectral measurements using a Nicolet Fourier transform infrared spectrometer and the L–I–V measurements were taken at 5-KHz repetition rate and 50-ns pulsewidth. All measurements were performed at a temperature of 80 K. QCLs with emission wavelengths of 4.9 and 9.8 μm were tested with a filling factor of 0.76, grating depths from 0.1 to 2.5 μm, and a grating period of $\lambda/\kappa n_f$, where $\kappa = 6$ and 18 for the 4.9- and 9.8-μm lasers, respectively, and is chosen such that $\Lambda \ll \lambda$ but large enough to be fabricated. In order to measure the effect of the grating on the facet reflectivity, these lasers were characterized before and after milling.

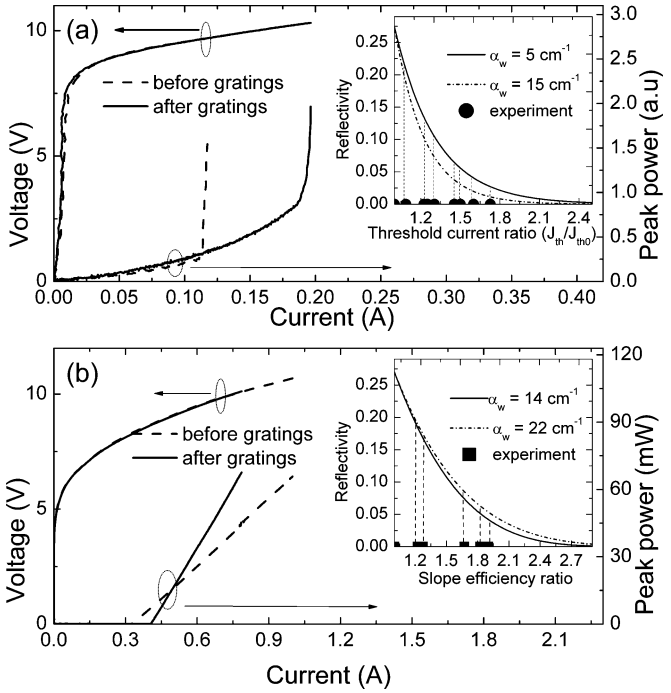

Fig. 2. L–I–V measurements showing the threshold shift and change in slope efficiency before and after milling the gratings. (a) $\lambda = 4.9\ \mu$m. The inset shows the reflectivity versus threshold current ratio, $L_{\rm cav} = 0.05$ cm for $\alpha_w = 5$ and 15 cm^{-1}. (b) $\lambda = 9.8\ \mu$m. The inset shows the reflectivity versus slope efficiency ratio, $L_{\rm cav} = 0.15$ cm for $\alpha_w = 14$ and 22 cm^{-1}.

In Fig. 2(a), the L–I–V characteristics for the 4.9-μm QCL measured with a cold InSb detector are shown. The inset depicts the calculated reflectivity versus threshold current ratio and the measured ratios. A similar plot was used for the 9.8-μm QCL. In Fig. 2(b), the L–I–V curves for $\lambda = 9.8\ \mu$m measured with a room-temperature HgCdTe detector are shown. The inset shows the calculated reflectivity versus the slope efficiency ratio for $\lambda = 9.8\ \mu$m and the measured ratios. The slope efficiency for $\lambda = 4.9\ \mu$m was not fully characterized because of the fast saturation of the cold detector used. Both L–I–V plots show an increase in the threshold current due to the gratings. In addition, Fig. 2(a) shows the spontaneous and amplified spontaneous emission which also increases; Fig. 2(b) shows in addition an increase in the slope efficiency. The reflectivity of the milled facet was determined by 1) taking the ratio of the threshold current density from the L–I–V data before $(J_{\rm th0})$ and after $(J_{\rm th})$ milling for different grating depths, and 2) projecting these ratios onto the simulated reflectivities given by (4) and shown in the insets. The same process is repeated with the slope efficiency.

In Fig. 3, the reflectivity versus the milled grating depth for the 9.8-μm QCL is shown. The inset presents the ratios obtained from the L–I–V plot for both 4.9- and 9.8-μm QCLs at different grating depths.

The far-field profile of the beam in the lateral direction (i.e., along the y-axis, see Fig. 1) and the transverse direction (along the x-axis), before and after milling the gratings, were also measured. In the lateral direction, a narrower profile of $\sim$10%, after milling the gratings, was observed. In the transverse direction, little change in the profile was observed.

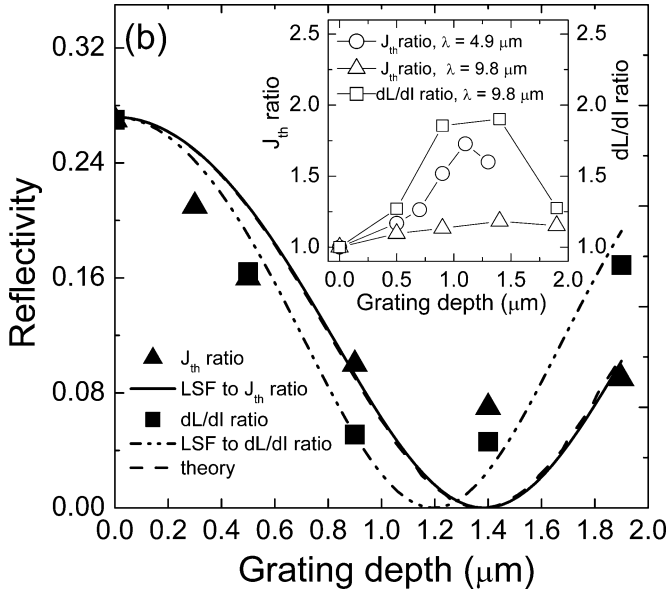

Fig. 3. Reflectivity versus the grating depth for $\lambda = 9.8\ \mu$m using $J_{\rm th}$ ratio and dL/dI ratio. LSF indicates the least squares fit to the data with n_f as the fit parameter in (2). The inset shows the experimental data of the threshold current ratio and slope efficiency ratio for different depths; the connecting lines serve as guides for the eyes.

IV. Discussion and Conclusion

For the 9.8-μm QCL, we simultaneously deduced the reflectivity from both the $J_{\rm th}$ ratio and dL/dI ratio. A loss range of 14–22 cm^{-1}, due to variations in the ridge width, ridge roughness, and imperfections, was measured using the Hakki–Paoli method [10]. This results in a minimum reflectivity range of 4%–8%. For the 4.9-μm QCL, we deduced the reflectivity from the $J_{\rm th}$ ratio. An expected loss range of 5–15 cm^{-1} results in a minimum reflectivity range of 1%–3%.

The reflectivities obtained from either the $J_{\rm th}$ ratio or dL/dI ratio experimentally do not easily go to zero. Possible reasons for this can be found in the following. First, the profile of the milled gratings (see inset of Fig. 1) does not quite match the rectangular profile assumed in theory. The profile is a result of the physical sputtering nature of the FIB such that for high aspect ratio, there is a significant amount of redeposition of the sputtered material back into the groove of the grating. Gas assisted etching is a method for reducing the effect of redeposition but this seriously reduces the resolution of the features that can be milled. A possible remedy to this is using electron beam lithography combined with dry chemical etching techniques to achieve better grating profile. Second, the emitted beam has a rather wide diverging angle which causes deviation from the normal incidence assumed in theory and needs to be corrected for.

We have shown that, using FIB for a first proof of principle, the reflectivity of QCL facets can be reduced to a few percent by etching subwavelength gratings into them.

Acknowledgment

The authors would like to thank Dr. N. Yao of the Imaging and Analysis Center (IAC) at Princeton University and A. Hoffman for his assistance with the far-field profile measurements.

References

[1] W. D'Oosterlinck, G. Morthier, M. K. Smit, and R. Baets, "Very steep optical thresholding characteristic using a DFB laser diode and an SOA in an optical feedback scheme," *IEEE Photon. Technol. Lett.*, vol. 17, no. 3, pp. 642–644, Mar. 2005.

[2] R. Maulini, M. Beck, J. Faist, and E. Gini, "Broadband tuning of external cavity bound-to-continuum quantum-cascade lasers," *Appl. Phys. Lett.*, vol. 84, pp. 1659–1661, Mar. 2004.

[3] R. Maulini, A. Mohan, M. Giovannini, and J. Faist, "External cavity quantum-cascade laser tunable from 8.2 to 10.4 μm using a gain element with a heterogeneous cascade," *Appl. Phys. Lett.*, vol. 88, pp. 201113_1–201113_3, May 2006.

[4] E. A. Zibik, W. H. Ng, D. G. Revin, L. R. Wilson, J. W. Cockburn, K. M. Groom, and M. Hopkinson, "Broadband $6\ \mu{\rm m} < \lambda < 8\ \mu$m superluminescent quantum cascade light-emitting diodes," *Appl. Phys. Lett.*, vol. 88, pp. 121109_1–121109_3, Mar. 2006.

[5] O. Stenzel, *The Physics of Thin Film Optical Spectra: An Introduction*. New York: Springer-Verlag, 2005, ch. 7.

[6] M. Born and E. Wolf, *Principles of Optics*. Cambridge, U.K.: Cambridge Univ. Press, 1997, pp. 54–74.

[7] T. K. Gaylord, W. E. Baird, and M. G. Moharam, "Zero-reflectivity high spatial-frequency rectangular-groove dielectric surface-relief gratings," *Appl. Opt.*, vol. 25, pp. 4562–4566, Dec. 1986.

[8] R. Brauer and O. Bryngdahl, "Design of antireflection gratings with approximate and rigorous methods," *Appl. Opt.*, vol. 33, pp. 7875–7882, Dec. 1994.

[9] C. Gmachl, F. Capasso, D. L. Sivco, and A. Y. Cho, "Recent progress in quantum cascade lasers and applications," *Rep. Prog. Phys.*, vol. 64, pp. 1533–1601, 2001.

[10] B. W. Hakki and T. L. Paoli, "Gain spectra in GaAs, double-heterostructure injection lasers," *J. Appl. Phys.*, vol. 46, pp. 1299–1306, 1975.